Soil surface moisture estimation over a semi-arid region using ENVISAT ASAR radar data for soil evaporation evaluation

M. Zribi, A. Chahbi, M. Shabou, Z. Lili-Chabaane, B. Duchemin, N. Baghdadi, R. Amri, A. Chehbouni

Hydrology and Earth System Sciences

Soil surface moisture estimation over a semi-arid region using ENVISAT ASAR radar data for soil evaporation evaluation

M. Zribi[1], **A. Chahbi**[1,2], **M. Shabou**[1,2], **Z. Lili-Chabaane**[2], **B. Duchemin**[1], **N. Baghdadi**[3], **R. Amri**[1,2], **and A. Chehbouni**[1]

[1]CESBIO (CNRS/IRD/UPS/CNES), UMR 5126, 18 avenue Edouard Belin, BPI 2801, 31401 Toulouse cedex 9, France
[2]INAT-LRSTE, 43, Avenue Charles Nicolle 1082, Tunis, Mahrajene, Tunisia
[3]UMR-TETIS, CEMAGREF, Montpellier, France

Abstract. The present paper proposes a method for the evaluation of soil evaporation, using soil moisture estimations based on radar satellite measurements. We present firstly an approach for the estimation and monitoring of soil moisture in a semi-arid region in North Africa, using ENVISAT ASAR images, over two types of vegetation covers. The first mapping process is dedicated solely to the monitoring of moisture variability related to rainfall events, over areas in the "non-irrigated olive tree" class of land use. The developed approach is based on a simple linear relationship between soil moisture and the backscattered radar signal normalised at a reference incidence angle. The second process is proposed over wheat fields, using an analysis of moisture variability due to both rainfall and irrigation. A semi-empirical model, based on the water-cloud model for vegetation correction, is used to retrieve soil moisture from the radar signal. Moisture mapping is carried out over wheat fields, showing high variability between irrigated and non-irrigated wheat covers. This analysis is based on a large database, including both ENVISAT ASAR and simultaneously acquired ground-truth measurements (moisture, vegetation, roughness), during the 2008–2009 vegetation cycle. Finally, a semi-empirical approach is proposed in order to relate surface moisture to the difference between soil evaporation and the climate demand, as defined by the potential evaporation. Mapping of the soil evaporation is proposed.

1 Introduction

Soil moisture is a key parameter, influencing the manner in which rainwater is shared between the phenomena of evapotranspiration, infiltration and runoff (Engman, 1991; Beven and Fisher, 1996; Koster et al., 2004). In the case of semi-arid and arid regions, this parameter is particularly important for irrigation management (Bastiaanssen et al., 2000). In order to optimise and protect water resources, which are often very limited, an accurate estimation of the soil's water content is needed, in order to determine the expected evapotranspiration flux. Considerable efforts are thus devoted to improving the evaluation of evapotranspiration, and to understanding its relationship with the vegetation cover and the soil's water content (Simonneaux et al., 2007). Soil evaporation estimations are essential in these regions, which are generally characterised by a dispersed vegetation cover associated with a strong contribution to the surface flux, following rainfall events in particular. Knowledge of the soil evaporation also allows the volume of water available for vegetation to be estimated. Several theoretical and experimental studies have already been published, dealing with the use of surface moisture for the estimation of evaporation. In the case of the land surface models, for example, the soil surface moisture is often considered to be the upper boundary condition (Bernard et al., 1986; Saux-Picart et al., 2009). These models require different parameterisations, and in particular the hydraulic conductivity or diffusivity between the surface and deeper layers. The difficulty in characterizing these parameters makes such approaches complex to use under operational conditions, or in regions with limited ground-truth measurements. The second type of approach relates the surface moisture estimation to the difference between soil evaporation and

Correspondence to: M. Zribi
(mehrez.zribi@ird.fr)

climatic demand. Various empirical relationships, relating the soil resistance to the surface soil moisture, have been proposed (Chanzy, 1991; Mahfouf and Noilhan, 1991; Chanzy and Bruckler, 1993; Simonneaux et al., 2009). Chanzy and Bruckler (1993) proposed an empirical model linking soil evaporation to soil moisture and climate demand, for different types of soil texture.

Concerning soil moisture estimation, over the last twenty years, radar remote sensing has demonstrated its strong potential (Ulaby et al., 1996; Moran et al., 2000; Le Hégarat-Mascle et al., 2002; Wagner et al., 2007). Using SAR observations, soil moisture can be estimated with a high spatial resolution, which is not the case with other types of remote sensing measurement (Jackson et al., 1996; Baup et al., 2007; Rahman et al., 2008).

The backscattered radar signal over bare soil strongly depends on soil moisture and surface roughness (Zribi et al., 2007; Baghdadi et al., 2007). In the case of sparse vegetation, the return signal depends both on the vegetation's backscattering characteristics, and on the attenuation it introduces to backscattering from the soil (Bindlish et al., 2001; Le Hégarat-Mascle et al., 2002). For bare soils, various theoretical and empirical approaches have been developed (Fung et al., 1992; Oh et al., 1992; Dubois et al., 1995; Zribi and Dechambre, 2002; Baghdadi et al., 2006; Thoma et al., 2008). Among these, the "linear approach" linking surface soil moisture to calibrated and validated SAR (Synthetic Aperture Radar) measurements (SIRC, ERS, RADARSAT, ASAR, TerraSAR-X, ... is widely used (Quesney et al., 2000; Zribi et al., 2007; Paris et al., 2010). The backscattered contribution from the vegetation is determined using physical or empirical models (Ulaby et al., 1986; Magagi and Kerr, 1997; Wigneron et al., 1999). Because of the high spatial variability of soil moisture in the studied region, resulting from variable convective phenomena causing the rainfall to be strongly localized in small areas, and as a consequence of the presence of a large fraction of irrigated areas, we propose a methodology in which soil moisture is estimated from SAR radar data. Our approach in this study is based on ASAR/ENVISAT radar data, acquired simultaneously with in situ measurements of surface parameters (moisture, roughness and vegetation). Two methodologies are proposed to map soil moisture over non-irrigated olive groves and wheat fields. Moisture estimations over olive groves are based, in particular, on a change-detection approach using ASAR/ENVISAT data, developed for the Sahel (Zribi et al., 2007). The methodology was broken down into several successive steps: (1) normalisation of radar data to one incidence angle equal to 20°, (2) for each cell, estimation of the areas with a low vegetation density, (3) elimination of surface roughness by subtracting the radar data recorded during the dry season from that used for the soil moisture determination, (4) retrieval of soil moisture, by inverting a linear relationship between the processed signals and the soil moisture. Moisture estimations over wheat fields are based on the

Fig. 1. Illustration of the studied site.

Cloud water model (Attema et al., 1978), using parameters estimated empirically from our database.

The present paper is organised as follows: Sect. 2 presents the data collected from the Kairouan plain region (Tunisia) under study: the database including satellite and ground-truth measurements is discussed. In Sect. 3, the proposed methodology for soil moisture retrieval is described. The derived results, including the validation of soil moisture estimations and mapping, are presented in Sect. 4. The evaluation of soil evaporation is discussed in Sect. 5. Finally, our conclusions are provided in Sect. 6.

2 Site description and ground-truth measurements

2.1 Site description

The Kairouan plain (Leduc et al., 2007) is situated in central Tunisia (9°30′ E–10°15′ E, 35° N, 35°45′ N) (Fig. 1). The climate in this region is semi-arid, with an average annual rainfall of approximately 300 mm per year, characterised by a rainy season lasting from October to May, with the two rainiest months being October and March. As is generally the case in semi-arid areas, the rainfall patterns in this area are highly variable in time and space. The mean temperature in Kairouan City is 19.2 °C (minimum of 10.7 °C in January and maximum of 28.6 °C in August). The mean annual potential evapotranspiration (Penman) is close to 1600 mm.

The landscape is mainly flat. The vegetation in this area is dominated by agriculture (cereals, olive trees, and market gardens). Crops are various and their rotation is typical of semi-arid regions. The aquifer of the Kairouan plain represents the largest basin in central Tunisia. It is fed by the infiltration of surface waters during floods in the natural regime,

Table 1. Characteristics of ENVISAT ASAR and SPOT data used in this study.

	Number	Pixel size	Mode/incidence angles	Polarisation/bands	Orbit
ENVISAT ASAR data	24	12.5 m × 12.5 m	Alternating polarisation Incidence angle: IS1, IS2, IS3	(HH, VV), HH	Ascending or descending
SPOT/HRV	10	10 m × 10 m	Incidence angle < 11°	Four bands B1: NIR B2: Red B3: Green B4: MIR	–

or at the time of dam releases since the construction of the Sidi Saad and El Haouareb dams. Surface and groundwater streams are drained into Sebkha Kelbia, a large salt lake.

2.2 Satellite data

2.2.1 Description

In March 2002, the European Space Agency launched the ENVISAT platform, carrying ASAR in its suite of instruments. Compared with ERS/SAR, this instrument has an extended measurement capacity, due to its multiple operating modes (Rosich, 2002). In particular, it has a greatly improved measurement repetition rate, with less than three days between two successive images taken at two different incidence angles, as opposed to a 35-day repeat cycle for ERS/SAR. In the present study, we chose to use the narrow observation mode, which generates high-resolution data (12.5 m × 12.5 m pixel spacing). Acquisitions were made between 2008 and 2010, at three different incidence angles (18° "IS1", 23° "IS2" and 27° "IS3") in co-polarized, alternating HH and VV polarization mode. Details of the SAR image characteristics are provided in Table 1. A large number of SPOT/HRV images was acquired simultaneously with the radar soundings. SPOT/HRV is a multi-spectral optical sensor, with two bands in the visible domain, one in the near infrared, and one in the medium infrared. These proved particularly useful for the mapping of land use and vegetation dynamics.

2.2.2 Data processing

Radar data

Absolute calibration of the ASAR images was carried out, to transform the radar signals (digitized values) into a backscattering coefficient ($\sigma°$). All images were geo-referenced using a geo-referenced SPOT/HRV image, resulting in an RMS control point error of about 10 m. The registration error of the ASAR images was taken into account in selecting Areas Of Interest (AOI) within each test field.

SPOT data

The SPOT/HRV images were firstly geo-referenced. Radiometric and atmospheric corrections were then applied in order to estimate the reflectance of the vegetation canopy. Finally, for each image, the Normalized Difference Vegetation Index (NDVI) was estimated. This index, given by the ratio between the difference between the visible and near-infrared channels, and the sum of these two channels, is related to the green vegetation photosynthetic activity (Rouse et al., 1973).

2.3 Ground truth measurements

Ground-truth measurements were carried out over different test fields, simultaneously to different satellite acquisitions. Ten test fields were selected for these measurements, to represent different types of land use: wheat fields (P4 – 2 ha, P6 – 1.5 ha, P7 – 6 ha, P9 – 3 ha and Pst2 – 2 ha), non-irrigated olive groves (P4bis – 6 ha), P10 – 2 ha, P12 – 6 ha), and bare soils (P5 – 2.5 ha). The studied site is characterised by the reduced size of most fields.

2.3.1 Surface moisture

Moisture measurements were taken simultaneously with the satellite acquisitions. The in situ collection of soil was extremely important in this experiment, as it was needed to validate the soil moisture retrieval algorithm. For each field, we made approximately twenty measurements, distributed over each field, at the time of each satellite acquisition. The distance between two successive measurement points was approximately 20 m. These were made using a handheld Thetaprobe, and by means of gravimetric measurements at depths between 0 and 5 cm. Thetaprobe measurements are calibrated with gravimetric measurements. Table 2 illustrates moisture values over field tests during different ground campaigns.

Table 2. Gravimetric volumetric soil moisture measurements (%) over test fields.

Field	P4	P4bis	P6	P7	P9	P10	P12	Pst2
23 December	–	6.26	6.11	7.23	6.3	5.78	5.9	–
16 January	31.65	23.68	16.4	32.04	18.62	17.7	17.56	–
21 January	40.43	36.15	34.77	39.64	33.75	28.34	28.57	–
31 January	28.65	21.17	18.91	29.7	18.07	14.55	18.8	–
6 February	21.38	18.63	18.28	20.67	14.86	12	–	17.56
18 February	15.61	14.97	14.57	16.98	13.2	12.15	11.5	16.35
25 February	14.07	14.1	12.96	15.97	11.5	10.94	8.43	–
4 March	20.57	11.2	8.98	24.85	11.75	–	–	20

Table 3. Roughness Rms height (cm) measurements.

Field	P4	P4bis	P6	P7	P9	P10	P12
24 March	0.8	2.5	0.8	0.6	0.7	1.5	1.6

2.3.2 Soil roughness

Roughness measurements were made using a pin profiler (total length of 1 m, and resolution of 2 cm). In order to guarantee suitable precision in the roughness computations, approximately 10 profiles were recorded for each field. As the surface height profile is considered to be ergodic and stationary, we can compute the correlation function for each profile (Zribi et al., 1997), and derive two statistical parameters: the rms height (vertical scale of roughness), and the correlation length (l) which represents the horizontal scale over which similar roughness conditions are detected. The rms height values are approximately equal to 0.7 cm for wheat fields, and are generally greater than 1.5 cm for olive groves, as illustrated in Table 3.

2.3.3 Vegetation covers

In order to characterise the vegetation covers, we considered three types of measurement. For the non-irrigated olive groves, we measured the distances between trees and the size of the trees in a large number of test fields. Distance between olive trees is of approximately 20 m, and the mean projected surface area of an adult olive tree, is approximately 16 m^2 (Fig. 2).

In the case of wheat fields, we implemented two types of measurement:

Leaf Area Index data

The Leaf Area Index (LAI) is defined as the total one-sided area of leaf tissue per unit ground surface area. According to this definition, the LAI is a dimensionless quantity

Fig. 2. View of a typical non-irrigated olive tree field.

characterizing the canopy of an ecosystem. During the 2008/2009 agricultural season, the LAI was derived from hemispherical digital photography based on analysis of the canopy gap fraction (Duchemin et al., 2008). These measurements were applied to each wheat field, on different days during the vegetation season. Irrigated wheat fields are generally characterised by a higher LAI than non-irrigated wheat fields. Before the end of March, the highest observed LAI was approximately 2. At the end of April we observed the highest vegetation density, with its maximum generally lying in the interval (4–6). Table 4 illustrates measurement values over wheat test fields.

Vegetation water content (VWC) data

The VWC was measured several times in five fields during the 2009 vegetation cycle (Table 4). For each field, measurements were made at three locations, each having a 1 m^2 surface area. The above ground biomass was removed, and wet and dry weights were used to compute the VWC. A mean value was computed from the three measurements.

Table 4. Leaf Area Index and vegetation water content measurement.

Field	P4		P6		P7		P9		Pst2	
	LAI	VWC (kg/m^2)	LAI	VWC (kg/m^2)	LAI	VWC (kg/m^2)	LAI	VWC (kg/m^2)	LAI	VWC (kg/m^2)
21 January		–		–		–	0.01	–		–
2 February	0.55	–	0.030	–	0.074	–	0.045	–	0.19	–
18 February	0.64	0.38	0.59	0.160	0.80	0.670	0.04	0.08	0.33	0.532
4 March	0.70	–	0.37	–	0.46	–	0.1	–	0.55	–
24 March	2.17	0.913	1.37	0.705	1.71	1.15	0.93	0.313	1.62	0.689
30 April	1.48	0.726	3.70	0.738	2.33	0.722	0.52	0.585	3.21	–

Land use

Land use validation was carried out in March 2009, with different fields being selected from the studied region (more than 150 fields) with two parts, a first one for the identification of empirical NDVI limits between different types of vegetation classes, and a second one for the validation of our approach to land use classification.

Land use mapping is based on a decision tree, using three types of satellite data: four SPOT images, SRTM data and finally two radar images. We established eight classes of land use: non-irrigated olive trees, irrigated olive trees, irrigated winter vegetables, irrigated summer vegetables, bare soils, urban areas, mountainous areas, water cover and areas of coastal salt flats "sebkhas". In the case of vegetables, as previously mentioned, we considered two classes, one for winter and the other for summer. We used empirical NDVI thresholds with the images acquired at the end of December 2008 (NDVI > 0.4) and during July 2009 (NDVI > 0.3). In fact, during these two periods, only irrigated vegetables presented a high NDVI. For the wheat classes (irrigated or non-irrigated), we made our analysis on two different dates, the first at the beginning of the cycle (in December 2008), and the second at the end of the vegetation development period (April 2009). The distinction between irrigated and non-irrigated wheat is based on a NDVI threshold equal to 0.5, since the irrigated class has a higher NDVI. Irrigated and non-irrigated olive trees are separated using a K-mean approach, based on a single optical SPOT image. The DTM provided by the Shuttle Radar Topography Mission (SRTM, http://srtm.usgs.gov/) allowed certain zones to be eliminated from our land use analysis. We excluded mountainous areas with an altitude greater than 300 m. We also identified water cover and urban classes. Validation of these remotely sensed classifications, based on ground verification over more than 100 fields with different types of land uses, reveals an accuracy of around 94%. Figure 3 illustrates the results of our land use mapping for the 2008–2009 season. The non-irrigated olive tree class covers 43% of the studied site, and the wheat class corresponds to 12% of the surface area of the studied site.
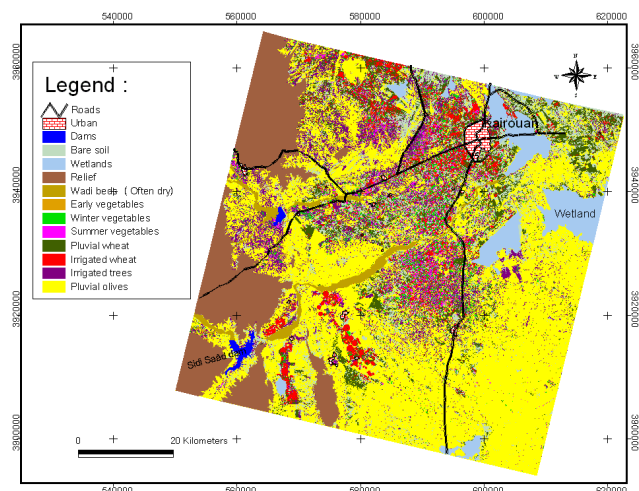

Fig. 3. Illustration of land use conditions during the 2008–2009 vegetation season.

3 Methodology of soil moisture estimation

Our approach to soil moisture estimation and mapping is carried out on two types of land use: Non-irrigated olive groves and wheat fields, which represent the two most important land use classes.

3.1 Soil moisture estimation over non-irrigated olive groves

Introduction

For the purposes of surface soil moisture estimation, we used the IS1, IS2, IS3 configurations, corresponding to low incidence angles of less than 30°. The aim of this approach was to limit the influence of vegetation and soil roughness, thereby increasing the accuracy of the moisture estimations.

The signal received from the non-irrigated olive groves can be written as the incoherent sum of two contributions (bare soil and vegetation cover), weighted by their respective percentages of terrain coverage. Using the estimated distance

between olive trees of approximately 20 m, and the mean projected surface area of an adult olive tree, i.e. approximately 16 m^2, we derive for different incidence angles lower than 30° a value between 4% and 10% for vegetation fraction. We propose to use the approach proposed by Zribi et al. (2007), detailed in introduction, and applied over disperse vegetation cove. The radar signal could be modelled with a linear relationship between radar signal and moisture, as:

$$\sigma^0_{\text{total}} \approx \alpha \ (\text{veg}) \ \times \ Mv + g \ (\text{Roughness, veg}) \tag{1}$$

Where α is related to vegetation fraction and to the attenuation due to the olive tree characteristics.

g is a function of soil roughness and vegetation cover effects on radar signal.

Mv is volumetric soil moisture.

The inversion process is based on three successive steps:

Normalisation of the radar signals to an incidence angle of 20°

Normalisation of the ASAR data is based on the interpretation of radar signal data, for different incidence angles, recorded over large olive tree AOIs. These areas are selected to be in the olive tree class, and only those radar images recorded on very dry dates are considered, in order to eliminate noise contributed by soil moisture effects. The angular dependence of backscattering coefficient is modelled with a mathematical function (Baghdadi et al., 2001) written as:

$$\sigma^0 = a \cos \ (\theta)^b \tag{2}$$

We retrieve b respectively equal to 5.5 and 6.3 for HH and VV polarisation.

Roughness and vegetation effect reduction

In order to limit roughness and vegetation effects, we consider a change-detection approach (Wagner et al., 1999; Moran et al., 2000; Zribi et al., 2007). We computed the difference between each raw data image and a reference image taken under dry conditions at the beginning of the vegetation season (21 December 2008), with a moisture content of approximately 5% over the studied site without spatial variations.

In the case of the olive groves, we observed very small variations during the vegetation cycle, due in particular to the olive trees being evergreen. We thus consider, as an initial hypothesis, that the vegetation has an approximately constant effect on the radar signal.

If we now consider a reference image, with a roughness R_1 and moisture content Mv_1 and a data image with a roughness R and moisture content Mv,

$$\Delta\sigma^0_{\text{total}} = \alpha(Mv - Mv_1) + g(\text{veg}, R) - g(\text{veg}, R_1) \tag{3}$$

As for surface roughness, the olive groves generally have a tillage corresponding to ploughed soil with an rms height

of around 1.5–3 cm, as shown in ground measurements. Only small variations could be observed after rainfall events. However, the soil is ploughed at different times during the year, which induces low variations on rms heights. For such roughness levels the backscattered radar signals are nearly saturated (Fung, 1994; Zribi et al., 1997). The subtraction of a reference image is therefore sufficient to considerably reduce the influence of roughness in the observed pixels, even for cases where there are small differences in roughness between the two images. We can thus simplify the above expression to:

$$\Delta \ \sigma^0_{\text{total}} \approx \alpha \ (Mv - Mv_1) + \varepsilon \tag{4}$$

Relationship between moisture and processed radar signals

Figure 4 illustrates the linear relationship found between a part of ground surface moisture measurements and radar signals over different test fields. Each point corresponds to a set of two measurements (ground-truth measurement, radar signal) recorded for different test fields. A strong correlation can be seen between the two types of data, for HH and VV polarisations, with a correlation coefficient R^2 equal to 0.67 and 0.53 respectively. The measured moisture contents range between 5% and 22%.

3.2 Moisture estimation over wheat fields

Introduction

Following an estimation of soil moisture related to precipitation effects, carried out over non-irrigated olive groves, we propose a second methodology over wheat fields. Because of limited fields scale (generally lower than 2ha), and high spatial variability of moisture between irrigated and non-irrigated wheat fields, we need to realize moisture estimation in higher spatial resolution.

In this case, the inversion algorithm is based on two steps:

Vegetation correction

In order to estimate the soil moisture over fields covered by vegetation, we first need to eliminate the vegetation's influence on the backscattered radar signal. We propose to use the water-cloud model developed by Attema and Ulab (1978). For an incidence angle θ, the backscatter coefficient is represented in the water cloud model by the expression:

$$\sigma^0 = \sigma^0_{\text{canopy}} + \sigma^0_{\text{canopy + soil}} + \tau^2 \ \sigma^0_{\text{soil}} \tag{5}$$

where τ^2 is the two-way vegetation transmissivity. The first term represents scattering due to the vegetation; the second term is linked to multiple scattering effects, and the third term represents the soil scattering attenuated by the vegetation cover. The second term can be neglected in the case of
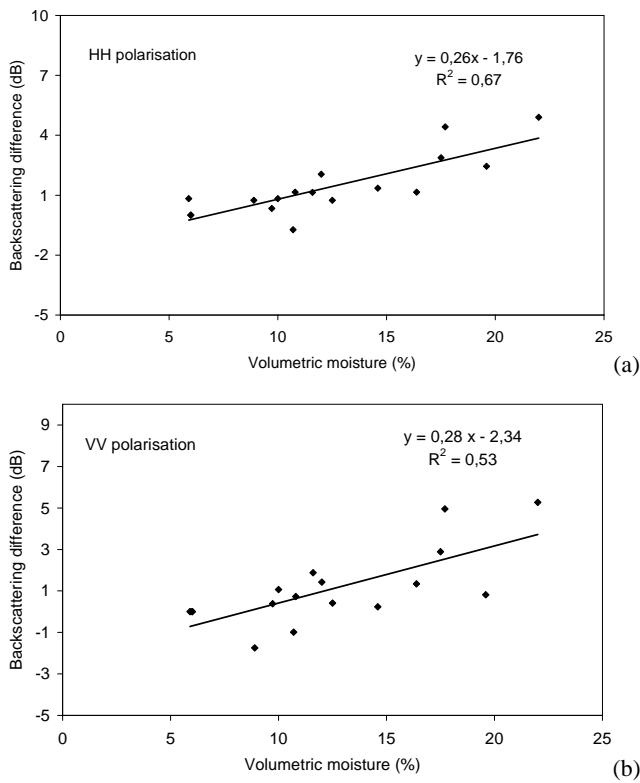
Fig. 4. Processed ENVISAT ASAR signals (in decibels) versus measured volumetric moisture over olive tree fields, **(a)** HH polarization, **(b)** VV polarization.

wheat scattering (Ulaby et al., 1986). Expression Eq. (5) can thus be simplified to:

$$\sigma^0 = \sigma^0_{canopy} + \tau^2 \, \sigma^0_{soil} \qquad (6)$$

with

$$\tau^2 = \exp\left(-2 \, B \,.\, \text{VWC} \,.\, \sec \theta \right) \qquad (7)$$

and

$$\sigma^0_{canopy} = A \,.\, \text{VWC} \,.\, \cos \theta \left(1 - \tau^2\right) \qquad (8)$$

where VWC is the vegetation water content (kg/m^2).

A and B are parameters which depend on the type of canopy. This formulation represents a first-order solution for the radiative transfer equation through a weak medium, where multiple scattering is neglected.

The database is divided into three sets: the first of these contains measurements acquired just before the vegetation starts to develop: from the end of December until the end of January, the soils are bare with no vegetation cover on the wheat fields. This set is used to estimate the backscattering contribution from bare soil. A second set is used to estimate the parameters of the radiative transfer model (A and B). Finally, a third set is used for model validation.

Relationship between soil moisture and bare soil radar signals

For bare soil backscattering, we consider a simple relationship between moisture and radar signal.

$$\sigma^0_{soil} (\theta) = \beta \, (\theta) \exp \left(\gamma \,.\, M_v\right) \qquad (9)$$

Where β is dependent on roughness and incidence angle, and γ corresponds to the slope of the moisture expressed as a function of the logarithm (dB) of the processed radar signal.

The slope γ is estimated using the first of the aforementioned database sets.

After sowing, the farmers do not till the soil again before harvesting. Our roughness ground measurements indicated the presence of smooth soils with an rms height approximately between 0.6 and 0.8 cm. It is reasonable to assume that for some wheat fields roughness could have a small decrease throughout our period of inversion. IEM simulations show approximately a 2 dB decrease of backscattering coefficient, at low incidence angles, for surfaces with a rms height going from 0.8 cm to 0.6 cm (Zribi and Dechambre, 2002). Our hypothesis of a constant mean β value for all wheat fields during period of inversion could then introduce a supplementary maximum error in volumetric moisture estimation of about 3% due to ±1 dB error in roughness effect.

4 Results and discussions of soil moisture estimation

4.1 Moisture estimation over olive trees

Validation of the proposed algorithm

Validation of the proposed algorithm is based on a comparison between a second part of ground-truth (gravimetric, and handheld Thetaprobe) measurements and estimations derived from ENVISAT ASAR data, for data acquired in 2010 and moisture conditions ranging from dry to wet, over the tested olive groves (P4bis, P10, P12). The resulting RMSE is equal to 3.8% for the HH and 4% for the VV polarisations, as illustrated in Fig. 5. Figure 6 illustrates a good coherence between soil moisture estimations with HH and VV radar signals, with an RMSE equal to 2% and bias equal to 1.6% over tested fields. The accuracy of this outcome demonstrates the robustness of the proposed algorithm, in spite of its simplicity. Our decision to develop an inversion algorithm, for olive trees only, considerably reduces the influence of roughness and vegetation on the soil moisture estimations. It is thus possible to apply this validated model to each ENVISAT ASAR image, to produce soil moisture maps over fields in the non-irrigated olive tree class.
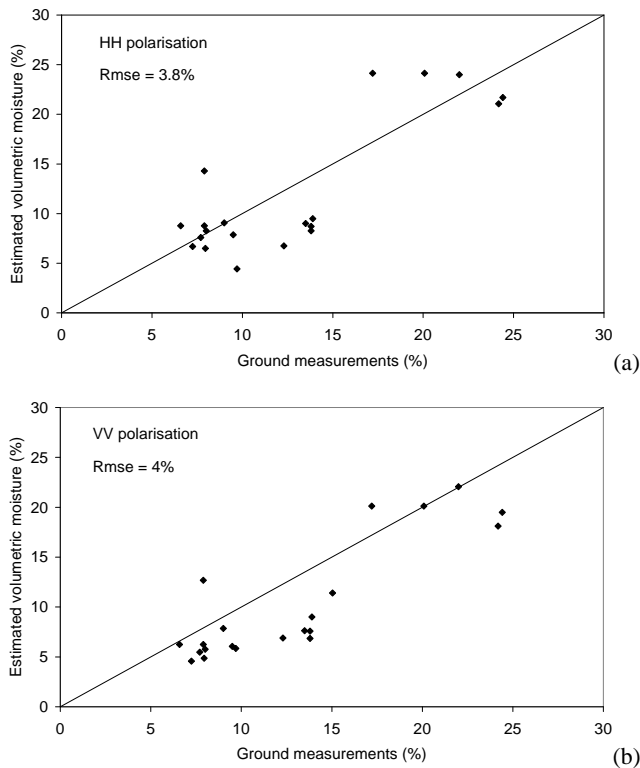
Fig. 5. Soil moisture estimations from ENVISAT ASAR data, expressed as a function of the soil moisture derived from ground-truth measurements, for fields in the "olive tree" class of land use, **(a)** HH polarisation, **(b)** VV polarisation.

Mapping of soil moisture

In order to eliminate the effects of local terrain heterogeneities (due to soil texture, vegetation dispersion heterogeneity, discontinuities between fields, etc) in the processed radar signal, the soil moisture was estimated over large cells defined by 100×100 pixel areas (about $1 \, \mathrm{km}^2$). For each resulting cell, the soil moisture estimation is applied only if more than 25% of the cell's pixels belong to olive groves. The value of the computed moisture can be then considered to be representative of the whole cell. To validate these estimations, the ground-truth measurements taken within the same cell are averaged. When the inversion is applied to the HH and VV radar signals, we observe similar results for both polarisations. In order to increase the precision of our estimations, we took the mean value of the two polarisations as the final result in the mapping process. In Fig. 7, soil moisture maps are shown for three different dates. These maps are directly related to the temporal and spatial variability of the precipitation over this region. For example, on date 9 December 2009, dry soil is observed over the full studied site, with a low moisture content of around 10%. Indeed, no rainfall was recorded during the 15 days preceding the acquisition of this satellite image. In the case of the image taken
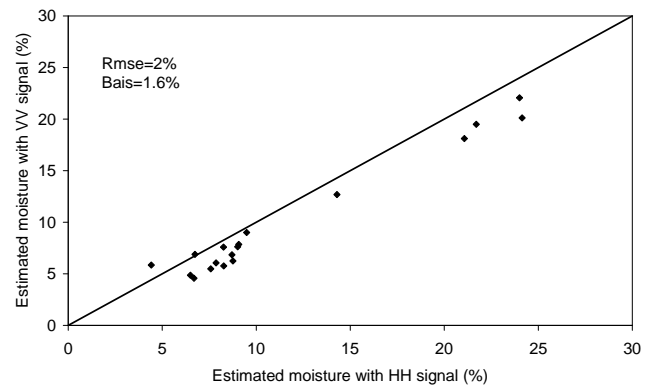

Fig. 6. Inter-comparison between HH and VV radar signal moisture estimations.

on 11 April 2009, strong spatial variability of the surface moisture can be observed. In fact, a rainfall event arriving from the West occurred during the afternoon of 11 April. In the Eastern part of this image, the soil moisture remained low. The third image in this figure provides the moisture map produced one day later, on 12 April, showing generalised rainfall throughout the studied site, associated with a global increase in soil moisture with a mean value of around 25%. Our approach allows the moisture to be estimated over approximately 50% of the studied site. It is presented particularly in the South East, where irrigated agriculture is absent. The interest of the choice of this class of land use is evident, since the computed moisture has only a small sensitivity to roughness and vegetation, both of which are affected by very limited changes from one year to another. This type of algorithm can thus be applied each year, with no need for it to be adapted to variations in local conditions.

4.2 Moisture estimation over wheat fields

Validation of moisture estimation

Validation of the proposed algorithm is based on comparisons between ground-truth measurements made in test wheat fields (P4, P6, P7, P9, Pst2) characterised by different soil moistures, ranging between dry and wet conditions and different vegetation development states, and estimations derived from ENVISAT ASAR radar signal acquisitions, made in 2009 and 2010. The results are illustrated in Fig. 8. We observe more validation points in HH polarisation because of the use of one ASAR image with just this configuration.

The resulting rms error is equal to 5.3% and 6.4%, in the respectively HH and VV polarisations. Although this accuracy could be considered to be adequate, in the case of irrigated fields we often observed a high spatial variation of the soil's moisture content. In addition, our measurements were often carried out within a three hour period before or after the site was overflown by the satellite. Some differences could arise due to a high evaporation rate, and in some cases it is
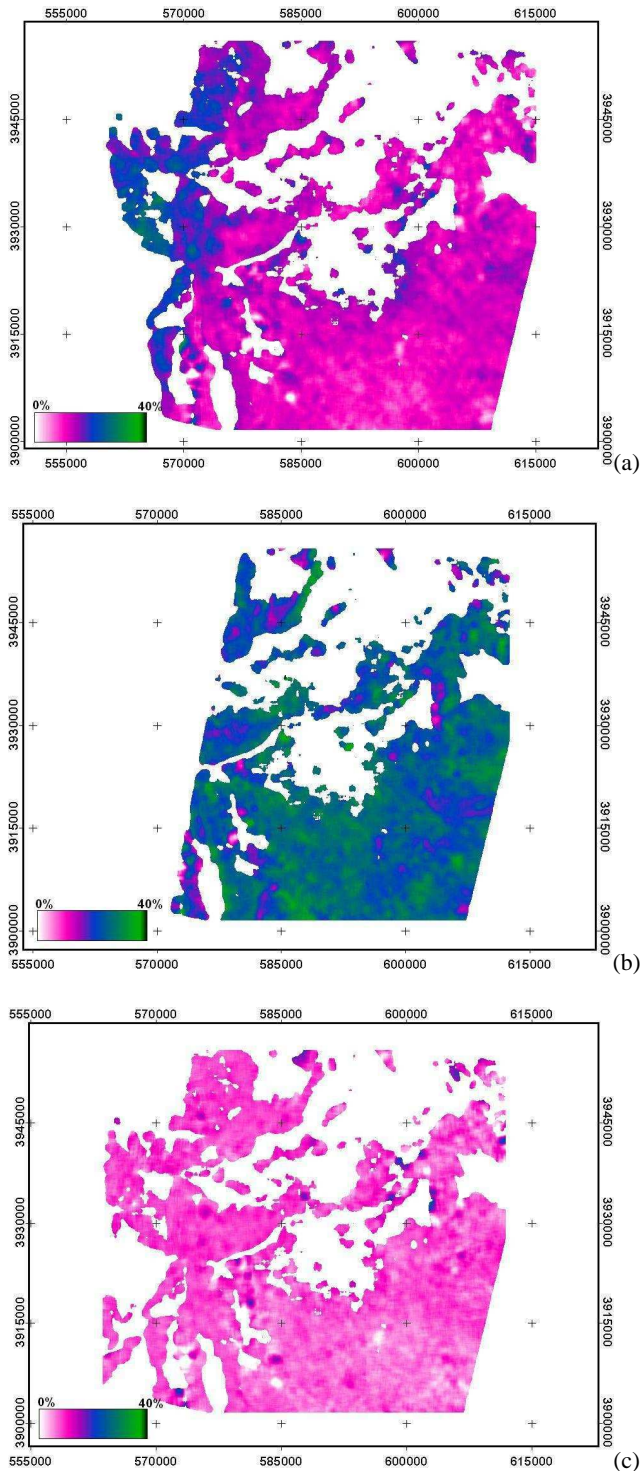
Fig. 7. Illustration of moisture mapping for an area containing fields in the "olive tree" class of land use, **(a)** 11 April 2009, **(b)** 12 April 2009, **(c)** 9 December 2009.
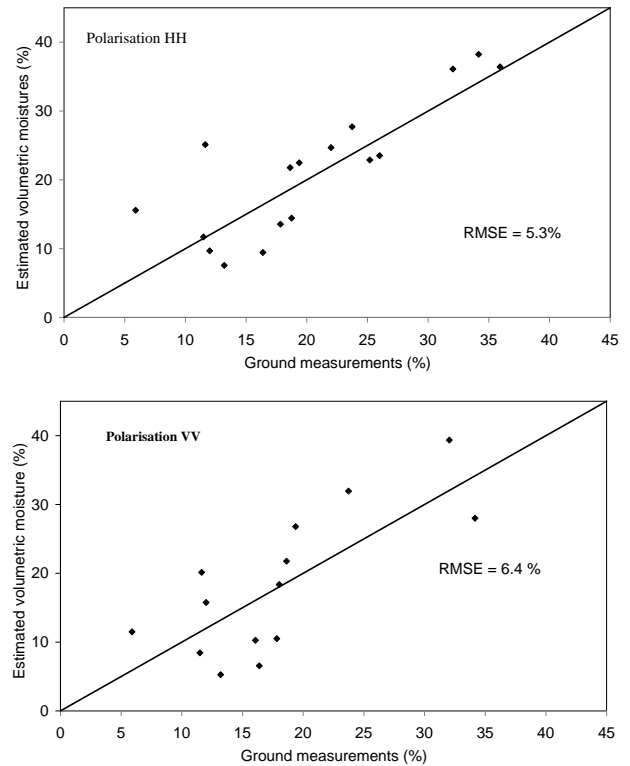

Fig. 8. Soil moisture estimations from ENVISAT ASAR data, versus soil moisture derived from ground truth measurements, for different test wheat fields.

possible that our ground-truth measurements were affected by irrigation which commenced during the satellite measurements. Finally, as discussed in the last section, the hypothesis of a constant roughness effect could increase the rms error.

Mapping of soil moisture over wheat fields

For the studied site, application of the inversion algorithm requires some information related to the vegetation's water content. For this reason, we developed an approach based on the interpretation of SPOT satellite optical measurements, linking VWC to LAI and then to NDVI index estimations.

Figure 9 illustrates the relationship between measurements of water content and LAI over different test fields. We observe a good correlation between the two variables, with R^2 equal to 0.61. Therefore, knowledge of the LAI values can be used to estimate the vegetation's water content (VWC), using the following equation:

$$\text{VWC} = 0.46\,\text{LAI} - 0.004 \tag{10}$$

For the LAI estimations, we made use of the NDVI vegetation index derived from SPOT images acquired during the full vegetation cycle. We proposed a relationship between NDVI and LAI estimations for wheat, based on a large database of ground and SPOT/HRV satellite measurements.
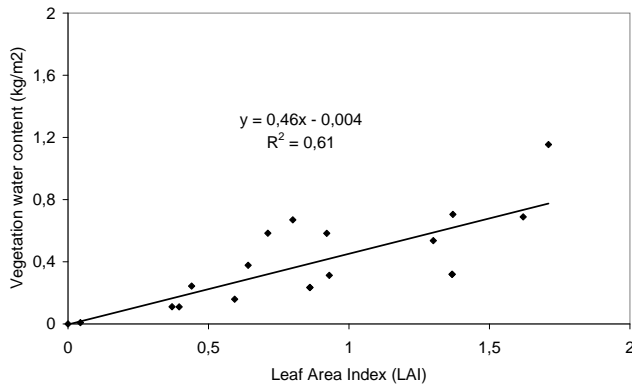
Fig. 9. Vegetation water content as a function of Leaf Area Index measured over wheat fields.

This expression is:

$$\text{NDVI} = \text{NDVI}_\infty + (\text{NDVI}_\text{soil} - \text{NDVI}_\infty) \times e^{-k\,\text{LAI}} \quad (11)$$

with $\text{NDVI}_\infty = 0.75$, $\text{NDVI}_\text{soil} = 0.15$ and $k = -1.24$.

For LAI < 2, we observe an increase in the LAI with NDVI indices. For higher values of LAI, the estimation becomes more complex, with saturation of the NDVI values resulting in reduced accuracy for the LAI estimations. In order to make reliable estimations of the vegetation moisture content, allowing accurate vegetation corrections, we ran the inversions only for the period between January and March, for which the LAI were still not high (lower than about 1.5). The expressions for water content estimation could then be applied with good accuracy. In the case of dense vegetation cover, it is very difficult to retrieve the soil moisture with sufficient precision. This is also an intrinsic limitation of the use of C-band SAR data, since the radar signal is strongly attenuated by the vegetation.

Our process thus involves, firstly NDVI mapping from SPOT satellite images, from which the LAI and then vegetation water content are deduced over wheat fields. Finally, after applying corrections for the influence of vegetation, we derive the soil moisture. All pixels in the wheat class of land use are considered to be valid candidates for soil moisture estimations. However, a radar signal from a minimum number of neighbouring pixels is required to avoid adding speckle noise to the results. We thus considered 5×5 pixel windows (about 0.4 ha) for the computation of effective radar signals in the wheat class, which were then used to estimate the soil moisture. Figure 10 illustrates the resulting soil moisture maps, computed over wheat fields at different dates. For wet days corresponding to rainfall events, such as that of 16 January 2009, a high soil moisture value can be observed for all wheat fields. For dry dates such as 7 March 2009, we observe different moisture values. Increasing moisture values can be observed over irrigated fields. On 24 December 2008 date, non-irrigated wheat fields are found to have soil moisture of approximately 6%. For irrigated wheat fields, the values are
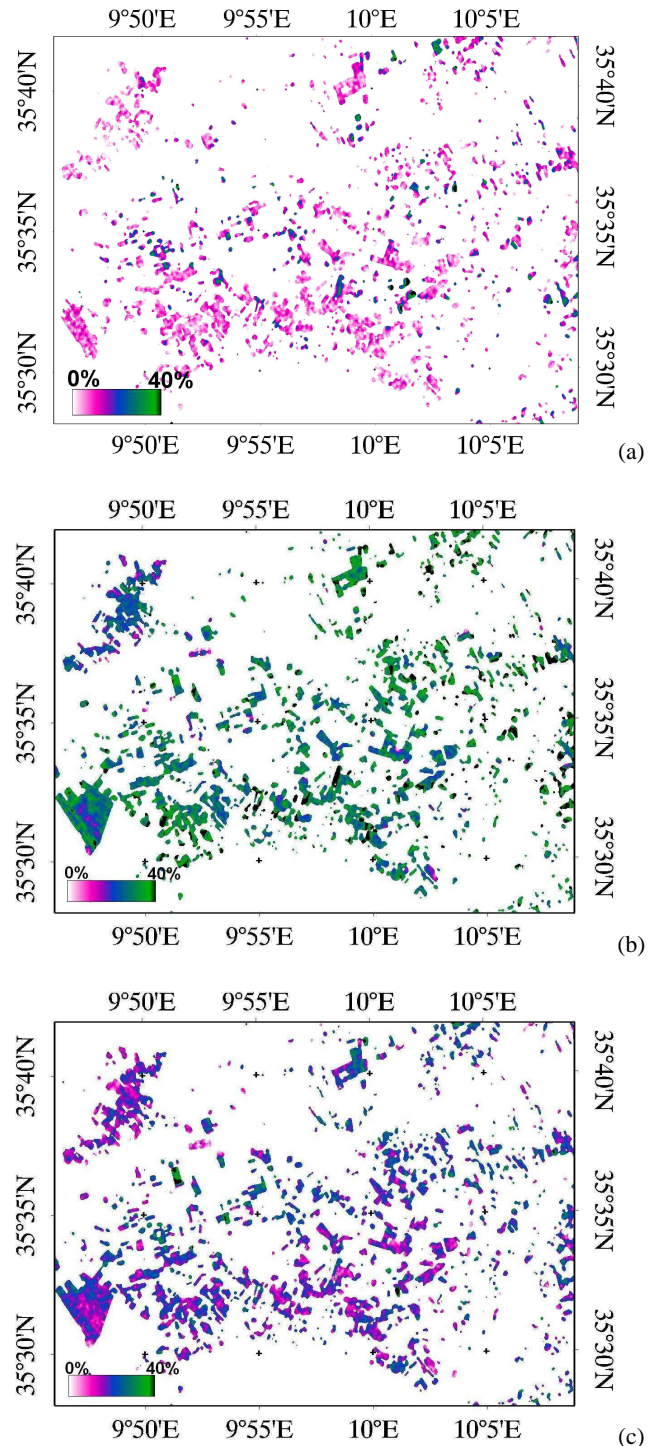

Fig. 10. Example of moisture mapping over wheat fields on three different dates: **(a)** 16 January 2009, **(b)** 20 Feburary 2009, **(c)** 27 March 2009.

generally higher; even very high moistures (around 40%) can be observed in some cases. The variability of these moisture observations is in complete agreement with the land use classification, distinguished by two classes, i.e. non-irrigated and irrigated wheat. This type of mapping process, if enhanced by means of high temporal monitoring, could become a very useful tool for the regional analysis of irrigation and water consumption, particularly in semi-arid areas with limited water resources.

4.3 Final moisture mapping

Figure 11 provides an illustration of our mapping process in a small area of our studied region, in 7 March 2009, in which moisture map computed for non irrigated olive groves and wheat fields are combined. Differences in moisture level can be observed between the two classes. The mean moisture level in the olive groves is approximately equal to 10%, as opposed to 15% for the wheat class fields. This difference is not due to irrigation alone, but also to differences in soil texture (for wheat fields – 45% clay, 26% silt and 39% sand, for olive groves – 29% clay, 8% silt, and 63% sand). With sandy soil, surface moisture decreases more rapidly after rainfall events.

5 Soil evaporation evaluation

5.1 Proposed methodology

As discussed in the introduction, the estimation of soil evaporation is essential in arid and semi-arid regions. In fact, for agriculture with a low density of vegetation cover, the contribution from soil evaporation is significant, particularly after rainfall events. An accurate estimation of this term thus allows a reliable estimation to be made of the stock of water available for use by the vegetation. In this section, we propose a simple approach for the estimation of soil evaporation.

Simonneaux et al. (2009) have proposed an integrating of the soil evaporation into a semi-empirical FAO evapotranspiration model (Allen et al., 2000), with a soil model represented with three layers: surface layer, root zone layer and a deeper layer. They consider the evaporation to be equal to ETP if surface layer is saturated. In this paper, we propose a simple approach for relating the soil evaporation to surface soil moisture (0–5 cm) estimated from radar satellite measurements. The soil evaporation can be written as:

$$\text{Es} = \left(\frac{Mv - Mv_i}{Mv_s - Mv_i} \right) . \text{ETP} \tag{12}$$

where Es is the soil evaporation, and ETP is the potential evaporation, which depends on climate demand and can be estimated using the FAO Penman-Monteith equation (Allen et al., 1998).
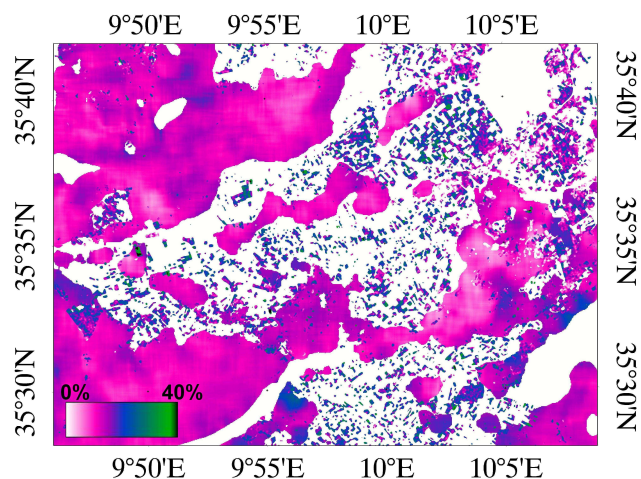

Fig. 11. Example of moisture mapping, showing soil moisture estimations for fields in the "olive tree" and "wheat" classes of land use on 7 March 2009.

Mv_i is the minimum soil surface moisture, as measured on the site. This is estimated from continuous ground thetaprobe measurements, acquired over a period of two years.

Mv_s is the soil saturation moisture. It is also estimated from continuous and spot ground measurements, acquired over a period of two years.

The soil evaporation is assumed to be at its maximum for saturated soils, with a value equal to the ETP. It is close to zero for very dry surfaces.

5.2 Application

In this section, we propose to generate a map of the soil evaporation, using retrieved soil moisture maps based on the inversion of ASAR/ENVISAT and ETP data acquired over the studied site.

Figure 12 illustrates the ETP variations during the 2008–2009 season, in which we observe a maximum during the summer season, with values of approximately 15 mm. The soil evaporation is however very low in this season, as a result of an absence of rainfall events, with surface soil moisture levels generally close to 0%. During the rainy season, as shown in Fig. 12, we observe a small number of rainfall events, followed by an increase in soil moisture. Thetaprobe continuous measurements show a drying process of the soil moisture lasting many days.

In the case of olive trees, we apply Expression Eq. (12) to each pixel of the moisture maps, without taking the vegetation cover fraction into account. In fact, soil evaporation takes place even directly beneath the olive trees. An Mv_s value of 28% is estimated for olive areas.

In the case of wheat fields, the soil evaporation is relevant only to the fraction without vegetation cover. The vegetation fraction Fc is estimated using the NDVI index retrieved from
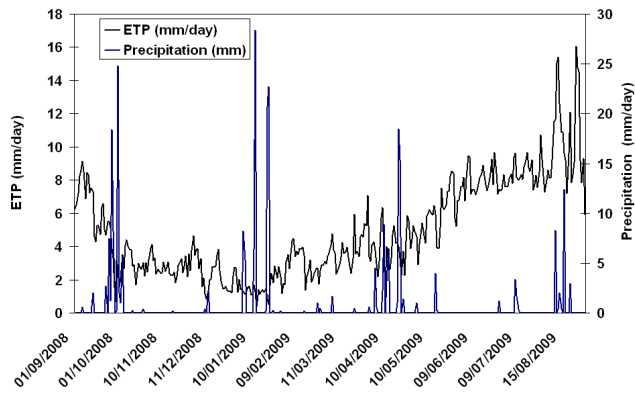
Fig. 12. Illustration of potential evapotransipration, calculated using Pennaman Monteith equation, during the agricultural season 2008–2009.

Fig. 13. Example of soil evaporation mapping over olive tree and wheat classes of land use on 7 March 2009.

SPOT vegetation data. We apply the relationship proposed by Er-Raki et al. (2007) over wheat fields in semi-arid areas. The soil evaporation can then be written as:

$$\mathrm{Es} = (1 - \mathrm{Fc}) \left(\frac{Mv - Mv_i}{Mv_s - Mv_i} \right) . \mathrm{ETP} \tag{13}$$

Mv_s value of 37% is estimated for wheat fields.

Figure 13 provides an example of soil evaporation mapping, on 7 March 2009. Particularly highest evaporation values can be observed over the olive fields without vegetation cover. The mean soil moisture over the olive groves is approximately 12%, and the soil evaporation is therefore approximately equal to 1.2 mm/day.

6 Conclusions

The objective of this paper was to propose a simple approach to evaluate soil evaporation using soil moisture retrievals from SAR radar measurements. Numerous studies have been published on the topic of soil moisture estimation over bare soil, or over land with one type of vegetation. The present study describes an approach for the mapping of soil moisture over two types of vegetation cover. The first of these concerns the "non-irrigated olive tree" land use class, dependent on rainfall events. A relationship is established between ground-truth measurements and backscattered radar signals. The proposed inversion approach is based on three main steps:

– Normalisation of the ENVISAT ASAR data to one incidence angle.

– Reduction of roughness effects through the subtraction of a reference image corresponding to a dry day.

– Implementation of an empirical relationship, enabling the soil moisture to be derived from the processed radar signals.
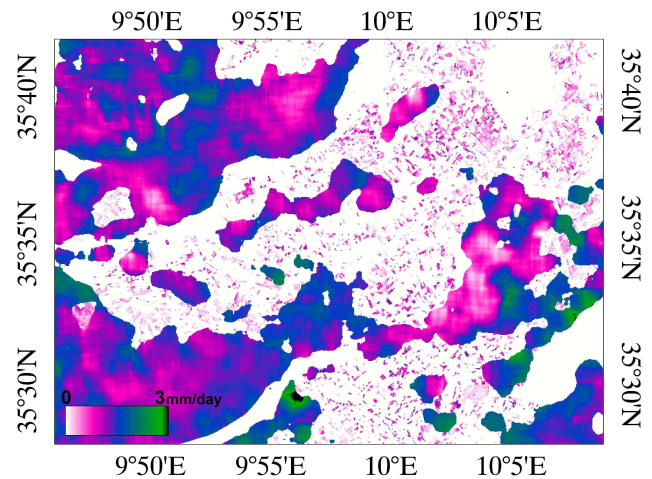
The validation of this approach has been demonstrated to have good accuracy in terms of moisture estimation. Moisture mapping using this process is shown for several dates, revealing various temporal and spatial variations, linked only to rainfall events. This estimation is proposed at a cell resolution of 100×100 pixels. The approach developed for fields in the non-irrigated olive tree class (about 43% of used land) allows nearly all areas of the studied region to be covered, from which a quantitative and precise estimation of the spatial variability of soil moisture can de derived.

A second type of moisture estimation is proposed over wheat fields. The principal objective of this estimation is to identify a relationship between moisture variability and irrigation in the studied region. The methodology developed for this application is based on two steps:

– Correction for vegetation effects using a simple first-order radiative transfer model. This correction is based on the relationships established between vegetation water content and optical satellite measurements (SPOT/HRV data).

– Determination of a linear relationship between ground moisture measurements and processed bare soil radar signals.

Good agreement is found between the inversion results and the ground-truth measurements, with a mean rms error of about 5.8%. Moisture mapping over wheat fields allows those fields that are irrigated, and thus characterised by generally higher moisture values, to be clearly identified, particularly during dry periods.

Finally, a semi-empirical approach is proposed for the evaluation and mapping of soil evaporation, using soil moisture estimations derived from radar measurements, and climate demand defined by potential evaporation. If this mapping process were associated with temporal monitoring at a

high repetition rate, it would make it possible to quantify the water stock available for the vegetation in rain-fed agriculture, characterised by a dominant non-covered surface, particularly during frequent periods of drought. In addition to the vegetation transpiration estimation, it would also allow the wheat fields' irrigation requirements to be monitored. Using ASAR/ENVISAT data, we can propose approximately one to two such estimations per week. With the arrival of new sensors, the SENTINEL-1 and RADARSAT constellations in particular, it will be possible to propose nearly daily estimations of soil evaporation which allows a high potential of surface moisture assimilation on land surface models.

Edited by: W. Wagner

The publication of this article is financed by CNRS-INSU.

References

Allen, R. G.: Using the FAO-56 dual crop coefficient method over an irrigated region as part of an evapotranspiration intercomparison study, J. Hydrol., 229, 27–41, 2000.

Allen, R. G., Pereira, L. S., Raes, D., and Smith, M.: Crop Evapotranspiration-Guidelines for Computing Crop Water Requirements, Irrigation and Drain, Paper No. 56, FAO, Rome, Italy, 300 pp., 1998.

Attema, E. P. W. and Ulaby, F. T.: Vegetation modeled as a water cloud, Radio Sci., 13, 357–364, 1978.

Baghdadi, N., Bernier, M., Gauthier, R., and Neeson, I.: Evaluation of C-band SAR data for wetlands mapping, Int. J. Remote Sens., 22(1), 71–88, 2001.

Baghdadi, N., Holah, N., and Zribi, M.: Soil moisture estimation using multi-incidence and multi-polarization ASAR SAR data, Int. J. Remote Sens., 27(8), 1907–1920, 2006.

Baghdadi, N., Aubert, M., Cerdan, O., Franchist'eguy, L., Viel, C., Martin, E., Zribi, M., and Desprats, J. F.: Operational mapping of soil moisture using synthetic aperture radar data: application to Touch basin (France), Sensors J., 7, 2458–2483, 2007.

Bastiaanssen, W. G. M., Molden, D. J., and Makin, I. W.: Remote sensing for irrigated agriculture: examples from research and possible applications, Agr. Water Manage., 46, 137–155, 2000.

Baup, F., Mougin, E., De Rosnay, P., Timouk, F., and Ch^enerie, I.: Surface soil moisture estimation over the AMMA Sahelian site in Mali using ENVISAT/ASAR data, Remote Sens. Environ., 109(4), 473–481, 2007.

Bernard, R., Soares, J. V., and Vidal Madjar, D.: Differential bare field drainage properties from airborne microwave observations, Water Resour. Res., 22, 869–875, 1986.

Beven, K. J. and Fisher, J.: Remote Sensing and Scaling in Hydrology, in: Scaling in Hydrology Using Remote Sensing, edited by: Stewart, J. B., Engman, E. T., Feddes, A., and Kerr, Y., Wiley, New York, 93–111, 1996.

Bindlish, R. and Barros, A. P.: Parameterization of vegetation backscatter in radar-based soil moisture estimation, Remote Sens. Environ., 76, 130–137, 2001.

Chanzy, A.: Modélisation simplifiée de l'évaporation du sol nu utilisant l'humidité et la température de surface accessibles par télédétection, Thèse de doctorat, p. 208, 1991.

Chanzy, A. and Bruckler, L.: Significance of soil surface moisture with respect to daily bare soil evaporation, Water Resour. Res., 29(4), 1113–1125, 1993.

Dubois, P. C., Van Zyl, J., and Engman, T.: Measuring soil moisture with imaging radars, IEEE T. Geosci. Remote, 33(4), 915–926, 1995.

Duchemin, B., Maisongrande, P., Boulet, G., and Benhadj, I.: A simple algorithm for yield estimates: Evaluation for semi-arid irrigated winter wheat monitored with green leaf area index, Environ. Modell. Softw., 23, 876–892, 2008.

Engman, E. T.: Applications of microwave remote sensing of soil moisture for water resources and agriculture, Remote Sens. Environ., 35(2–3), 213–226, 1991.

Er-Raki, S., Chehbouni, A., Guemouria, N., Duchemin, B., Ezzahar, J., and Hadria, R.: Combining FAO-56 model and ground-based remote sensing to estimate water consumptions of wheat crops in a semi-arid region, Agr. Water Manage., 87, 41–54, 2007.

Fung, A. K., Li, Z., and Chen, K. S.: Backscattering from a randomly rough dielectric surface, IEEE T. Geosci. Remote, 30(2), 356–369, 1992.

Fung, A. K.: Microwave scattering and emission models and their applications, Artech House, Boston, MA, 1994.

Jackson, T.-J., Schmugge, J., and Engman, E.-T.: Remote sensing applications to hydrology: soil moisture, Hydrol. Sci., 41(4), 517–530, 1996.

Koster, R. D., Dirmeyer, P. A., Guo, Z., Bonan, G., Chan, E., Cox, P., Gordon, C. T., Kanae, S., Kowalczyk, E., Lawrence, D., Liu, P., Lu, C. H., Malyshev, S., McAvaney, B., Mitchell, K., Mocko, D., Oki, T., Oleson, K., Pitman, A., Sud, Y. C., Taylor, C. M., Verseghy, D., Vasic, R., Xue, Y., and Yamada, T.: Regions of Strong Coupling Between Soil Moisture and Precipitation, Science, 305, 1138–1140, doi:10.1126/science.1100217, 2004.

Le Hégarat-Mascle, S., Zribi, M., Alem, F., Weisse, A., and Loumagne, C.: Soil moisture estimation from ERS/SAR data: Toward an operational methodology, IEEE T. Geosci. Remote, 40(8), 1–12, 2002.

Leduc, C., Ben Ammar, S., Favreau, G., B'eji, R., Virrion, R., Lacombe, G., Tarhouni, J., Aouadi, C., Zenati Chelli, B., Jebnoun, N. O. M., Michelot, J. L., and Zouari, K.: Impacts of hydrological changes in the Mediterranean zone: environmental modifications and rural development in the Merguellil catchment, central Tunisia, Hydrolog. Sci. J., 52(6), 1162–1178, 2007.

Magagi, R. D. and Kerr, Y. H.: Retrieval of soil moisture and vegetation characteristics by use of ERS-1 wind scatterometer over arid and semi-arid areas, J. Hydrol., 188–189, 361–384, 1997.

Mahfouf, J. F. and Noilhan, J.: Comparative study of various formulations of evaporation from bare soil using in-situ data, J. Appl. Meteorol, 30(7), 1354–1365, 1991.

Moran, M. S., Hymer, D. C., Qi, J., and Sano, E. E.: Soil moisture evaluation using multitemporal synthetic aperture radar (SAR) in semiarid rangeland, Agr. Forest Meteorol., 105, 69–80, 2000.

Oh, Y., Sarabandi, K., and Ulaby, F. T.: An empirical model and an inversion technique for radar scattering from bare soil surfaces, IEEE T. Geosci. Remote, 30(2), 370–381, 1992.

Paris, A. T., Zribi, M., Baghdadi, N., and Loumagne, C.: Analysis of local variation of soil surface parameters with TerraSAR-X radar data over bare agricultural fields, IEEE T. Geosci. Remote, 48(2), 874–881, 2010.

Quesney, A., Le H'egarat-Mascle, S., Taconet, O., Vidal-Madjar, D., Wigneron, J. P., Loumagne, C., and Normand, M.: Estimation of watershed soil moisture index from ERS/SAR data, Remote Sens. Environ., 72, 290–303, 2000.

Rahman, M. M., Moran, M. S., Thoma, D. P., Bryant, R., Holifield-Collins, C. D., Jackson, T., Orr, B. J., and Tischler, M.: Mapping surface roughness and soil moisture using multi-angle radar imagery without ancillary data, Remote Sens. Environ., 112, 391–402, 2008.

Rosich, B.: ASAR Validation Review, ESRIN, Frescatti, 11–12 December, 2002.

Rouse, J. W., Haas, R. H., Schell, J. A., and Deering, D. W.: Monitoring vegetation systems in the great plains with ERTS, Third ERTS Symposium, NASA SP-351 I, 309–317, 1973.

Saux-Picart, S., Ottlé, C., Perrier, A., Decharme, B., Coudert, B., Zribi, M., Boulain, N., Cappelaere, B., and Ramier, D.: SEtHyS_Savannah: a multiple source land surface model applied to sahelian landscapes, Agr. Forest Meteorol., 149(9), 1421–1432, 2009.

Simonneaux, V., Duchemin, B., Helson, D., ER-Raki, S., Olioso, A., and Chehbouni, A. G.: The use of high-resolution image time series for crop classification and evapotranspiration estimate over an irrigated area in central Morocco, Int. J. Remote Sens., 29(1–2), 95–116, doi:10.1080/01431160701250390, 2007.

Simonneaux, V., Lepage, M., Helson, D., Metral, J., Thomas, S., Duchemin, B., Cherkaoui, M., Kharrou, H., Berjami, B., and Chehbouni, A.: Estimation spatialisée de l'évapotranspiration des cultures irriguées par télédétection : application à la gestion de l'irrigation dans la plaine du Haouz (Marrakech, Maroc), Sécheresse, 20(1), 123–130, 2009.

Thoma, D. P., Moran, M. S., Bryant, R., Rahman, M. M., Holifield Collins, C. D., Keefer, T. O., Noriega, R., Osman, I., Skrivin, S. M., Tischler, M. A., Bosch, D. D., Starks, P. J., and Peters-Lidard, C. D.: Appropriate scale of soil moisture retrieval from high resolution radar imagery for bare and minimally vegetated soils, Remote Sens. Environ., 112(2), 403–414, 2008.

Ulaby, F. T., Moore, R. K., and Fung, A. K.: Microwave Remote Sensing Active and Passive, Artech House, Inc., Addison-Wesley, Reading, MA, 1986.

Ulaby, F. T., Dubois, P. C., and van Zyl, J.: Radar mapping of surface soil moisture, J. Hydrol., 184(1/2), 57–84, 1996.

Wagner, W., Lemoine, G., and Rott, H.: A method for estimating soil moisture from ERS Scatterometer and soil data, Remote Sens. Environ., 70, 191–207, 1999.

Wagner, W., Bloschl, G., Pampaloni, P., Calvet, J.-C., Bizzarri, B., Wigneron, J.-P., and Kerr, Y.: Operational readiness of microwave remote sensing of soil moisture for hydrologic applications, Nord. Hydrol., 38, 1–20, 2007.

Wigneron, J. P., Ferrazzoli, P., Olioso, A., Bertuzzi, P., and Chanzy, A.: A Simple Approach To Monitor Crop Biomass from C-Band Radar Data, Remote Sens. Environ., 69(2), 179–188, 1999.

Zribi, M. and Dechambre, M.: A new empirical model to retrieve soil moisture and roughness from Radar Data, Remote Sens. Environ., 84(1), 42–52, 2002.

Zribi, M., Taconet, O., Le Hégarat-Mascle, S., Vidal-Madjar, D., Emblanch, C., Loumagne, C., and Normand, M.: Backscattering behavior and simulation comparison over bare soils using SIRC/XSAR and ERASME 1994 data over Orgeva, Remote Sens. Environ., 59(2), 256–266, 1997.

Zribi, M., Saux-Picart, S., André, C., Descroix, L., Ottlé, O., and Kallel, A.: Soil moisture mapping based on ARSAR/ENVISAT radar data over a sahelian site, Int. J. Remote Sens., 28(16), 3547–3565, 2007.

Hydrol. Earth Syst. Sci., 15, 345–358, 2011

www.hydrol-earth-syst-sci.net/15/345/2011/